Front. Mater. Sci. 2022, 16(1): 220587
https://doi.org/10.1007/s11706-022-0587-7

RESEARCH ARTICLE

Facile and scalable preparation of ultra-large boron nitride nanosheets and their use for highly thermally conductive polymer composites

Wenyu WU[1], Bin GUO[1], Xiaojing LIU[1], Huaxin MA[1], Zhao ZHANG[1], Zhi ZHANG[1], Minghao CUI[1], Yu GU[2], and Ruijun ZHANG (✉)[1]

1 State Key Laboratory of Metastable Materials Science and Technology, Yanshan University, Qinhuangdao 066004, China
2 Academic Affairs Office, Tangshan Normal University, Tangshan 063000, China

ABSTRACT: Due to their excellent physical and chemical properties, boron nitride nanosheets (BNNSs) have shown great application potential in many fields. However, the difficulty in scalable preparation of large-size BNNSs is still the current factor that limits this. Herein, a simple yet efficient microwave-assisted chemical exfoliation strategy is proposed to realize scalable preparation of BNNSs by using perchloric acid as the edge modifier and intercalation agent of h-BN. The as-obtained BNNSs behave a thin-layered structure (average thickness of 3.9 nm) with a high yield of ~16%. Noteworthy, the size of BNNSs is maintained to the greatest extent so as to realize the preparation of BNNSs with ultra-large size (up to 7.1 μm), which is the largest so far obtained for the top-down exfoliated BNNSs. Benefiting from the large size, it can significantly improve the thermal diffusion coefficient and the thermal conductivity of polyvinyl alcohol by 51 and 62 times respectively, both showing a higher value than the one previously reported. This demonstrates that the prepared BNNSs have great promise in enhancing the thermal conductivity of polymer materials.

KEYWORDS: boron nitride nanosheet; thermal conductivity; chemical exfoliation; large size

Contents

Received October 12, 2021; accepted December 25, 2021

E-mail: zhangrj@ysu.edu.cn

1 Introduction

The use of miniaturized, highly integrated and high-power density electronic devices will result in the generation of a large amount of heat, and the continuous accumulation of heat will seriously affect their performance and service life [1–3]. Therefore, this puts forward higher requirements for the development of high-performance thermal management materials. Among them, polymer-based

composite materials have been widely used in the field of microelectronic packaging due to their low cost, processability, electrical insulation, light weight, flexibility, etc. [4–5]. However, the thermal conductivity of polymers in general is not ideal (about 0.2 $W \cdot m^{-1} \cdot K^{-1}$), so fillers with high thermal conductivity such as graphene, aluminum nitride, carbon nanotubes, and boron nitride (BN) need to be added to enhance its thermal conductivity [6–9].

Hexagonal boron nitride (h-BN), a similar structure to graphite, has been widely used as the attractive thermally conductive filler due to its high thermal conductivity, electrical insulation, and corrosion resistance [10–12]. Compared with bulk h-BN (400 $W \cdot m^{-1} \cdot K^{-1}$), boron nitride nanosheets (BNNSs) with a two-dimensional (2D) structure show higher thermal conductivity (600 $W \cdot m^{-1} \cdot K^{-1}$) due to the reduction of phonon–phonon scattering with decreasing the number of layers [13], and the thin-layer structure of BNNSs is more conducive to the formation of heat conduction network in the polymer [14–15]. In addition, as an important parameter to improve the thermal conductivity of polymers, the lateral size of BNNSs also plays a vital role [13]. BNNSs with the small lateral size will usually significantly increase the interfacial thermal resistance, resulting in a lower thermal conductivity of the composites [16–17]. In general, the realization of the scalable preparation of large-size BNNSs is particularly important to better meet its application requirement.

Up to now, many strategies have been developed for the preparation of BNNSs. Generally speaking, these preparation strategies can be classified into two major categories according to their production mechanisms: the bottom-up route and the top-down route [18]. The former mainly relies on the high-temperature treatment of various precursors on substrates to form few-layered BNNSs [19]. However, some challenging issues, including high cost and complex hardware systems, limit their practical applications. The latter is mainly based on the exfoliation of bulk h-BN, which is performed via utilizing additional mechanical or chemical force to the h-BN layer to overcome the van der Waals forces [20–21]. However, the higher exfoliation energy of h-BN, which is ~33% higher than that of graphite due to the smaller distance and the 'lip−lip' interactions between h-BN layers [22], directly makes it more difficult to be exfoliated into BNNSs with large lateral size. For example, as a commonly-used strategy for the exfoliation of h-BN, liquid-phase exfoliation of h-BN to few-layer BNNSs can be realized with the assistance of the mechanical external force generated from an ultrasonicator. However, usually the lateral size of BNNSs obtained is very small (mostly $\leqslant 1$ μm), since the h-BN sheets can be easily broken up into little fragments under ultrasonic treatment [23–24]. Ball-milling can also exfoliate the bulk h-BN into few-layered BNNSs. Nevertheless, the violent collision between milling balls and bulk h-BN results in a significant decrease in the lateral size of the as-prepared BNNSs, which ranges from tens to hundreds of nanometers only [25–26]. By comparison, the chemical treatment seems more advantageous in the preparation of larger-size BNNSs, since the chemical reagents can modify the edge structure of h-BN or expand its interlayer spacing by introducing foreign substances, which is beneficial to further realize the effective exfoliation of h-BN [27–28]. For example, Yuan et al. introduced hydroxyl functional groups at the edge of h-BN by potassium hydroxide pretreatment and further expanded the interlayer spacing of h-BN by means of low-temperature hydrogen annealing. As a result, the average lateral size of the obtained BNNS by exfoliating the treated h-BN can reach 1.6 μm [17]. Also, a modified Hummers' chemical treatment route for the exfoliation of h-BN was reported by Du et al. [29]. Although the resultant lateral size of the BNNSs is up to micron level (~3 μm), the long reaction period, pollution of heavy metal ions (e.g., Mn^{2+}) and complicated preparation process will greatly limit its practical application. Thus, the facile and scalable methods for the high efficiency production of BNNSs with large lateral size are still urgently desired.

Herein, we present a facile and cost-effective microwave-assisted chemical method to produce few-layer BNNSs with large lateral size. In this method, the bulk h-BN is soaked in perchloric acid ($HClO_4$) to modify the edge of h-BN and insert into the h-BN layer. Then, a short-time microwave treatment on the soaked h-BN leads the exfoliation of h-BN to few-layer BNNSs. Interestingly, the obtained BNNSs have an ultra-large lateral size (the maximum lateral size can be up to 16 μm, and the average sheet lateral size is 7.1 μm). When added into polyvinyl alcohol (PVA), BNNSs can greatly improve the thermal conductivity of PVA, demonstrating that the prepared large-size BNNSs have a great application potential for improving the thermal conductivity of polymer materials.

2 Experimental

2.1 Preparation of BNNSs

Firstly, 0.4 g h-BN powder (mean particle size of about

15 μm) and 10 mL $HClO_4$ (72%) were completely mixed in a 50 mL flask by stirring for 30 min at room temperature. Subsequently, the exfoliation of h-BN would be carried out in two steps, including a pre-soaking step and a microwave-heating step. In the pre-soaking step, the flask was transferred into an oil bath at 180 °C and stayed for 10 h under magnetic stirring. At this time, the obtained BN product was labeled BN-180. In the microwave (MW)-heating step, the mixed solution of $HClO_4$ containing BN-180 was transferred into a quartz beaker, and then immediately MW-irradiated for ~6 min with a 700 W ordinary household MW oven (provided by Media, China). During the MW irradiation period, a large amount of gases would be generated, resulting in the exfoliation of h-BN (denoted as exf-BN).

In order to separate the obtained BNNSs and calculate its exfoliation yield, 0.1 g exf-BN was added into 100 mL isopropanol (IPA) and sonicated for 30 min to obtain a uniform dispersion. The dispersion was centrifuged at a speed of 600 $r \cdot min^{-1}$ for 10 min, then the supernatant was poured out carefully, and an appropriate amount of IPA was continued to be added into the precipitate, repeating the ultrasonic dispersion and centrifugation process until the supernatant was colorless. Among them, the product in the supernatant portion (denoted as BNNSs) was used for further characterization. The unexfoliated h-BN (mark its mass as m_1, unit: g) at the bottom was dried at 60 °C for 24 h, which is used to calculate the exfoliation yield (η):

$$\eta/\% = \frac{0.1 - (m_1/\mathrm{g})}{0.1} \times 100 \quad (1)$$

Moreover, in order to compare the products obtained under different reaction conditions, samples that were pre-soaked in $HClO_4$ for 0, 5 and 15 h were also prepared and labeled as BNNS-0, BNNS-5 and BNNS-15, respectively, with other conditions remaining unchanged. Meanwhile, samples obtained by the pre-soaking process in $HClO_4$ for 10 h as well as the MW-heating treatment for only 3 min were labeled as BNNS-3MW.

2.2 Preparation of PVA/BNNS composite films

Typically, a 5 wt.% PVA solution was firstly prepared by dissolving PVA in deionized water under magnetic stirring at 90 °C for 2 h. The BNNS dispersion (1 $mg \cdot mL^{-1}$) was prepared by adding BNNS powders in the IPA solution, followed by the sonication for 0.5 h. Subsequently, the dispersion was vacuum-filtered to make BNNSs uniformly deposited on the poly(tetrafluoroethylene) (PTFE) membrane (47 mm in diameter, 0.22 μm in pore size) to form the disk-shape BNNS specimen. Then, 3 mL of the PVA solution was gently added onto the BNNS specimen and dried in an oven at 60 °C for 8 h. Finally, the PVA/BNNS composite film was peeled off directly from the membrane filter. To investigate the effect of the BNNS content, different PVA/BNNS composite films with the BNNS contents of 0, 15, 25, 35, and 45 wt.% were prepared, denoted as PVA/BNNS-0, PVA/BNNS-15, PVA/BNNS-25, PVA/BNNS-35, and PVA/BNNS-45, respectively. For comparison, PVA/h-BN-35 composite films with 35 wt.% h-BN as the filler were also prepared by using the same film-making method.

2.3 Characterization

Fourier transform infrared spectroscopy (FTIR) was performed by a Fourier transform infrared spectrometer (E55Xfra106, BRUKER, Germany). X-ray diffraction (XRD) study was carried out at a Rigaku D/MAX-2500 powder diffractometer with Cu Kα radiation ($\lambda = 0.154$ nm) operated at 40 kV and 200 mA, and Raman spectra were recorded via a Renishaw inVia Raman microscope with a laser wavelength of 532 nm. X-ray photoelectron spectroscopy (XPS) was performed by using a K-alpha spectrometer (Thermo VG Corporation, USA) with the Al Ka radiation (1486.6 eV, 15 kV). The morphology and the microstructure of h-BN, BN-180 and BNNSs were characterized by field-emission scanning electron microscopy (FESEM; Hitachi S-4800, operated at 15 kV), transmission electron microscopy (TEM; JEOL JEM-2010, operated at 200 kV), and atomic force microscopy (AFM; Bruker-Multi Mode 8). Tensile tests were performed on a universal tester (CMT6103, China) with a strain rate of 4 $mm \cdot min^{-1}$. The thermal diffusivity (α) values of PVA/BNNS composite films were detected by using a laser-flash diffusivity instrument LFA 467 (NETZSCH, Germany). The density (ρ) values of composite films were obtained by using a micrometer for dimensional measurements and a microbalance for weight measurements. The specific heat capacity (c) values of composite films were detected from differential scanning calorimetry (DSC; 200 F3, NETZSCH, Germany). Both the thermal diffusivity and the specific heat capacity were characterized at room temperature. The thermal conductivity (κ) was calculated from the equation: $\kappa = \alpha \times \rho \times c$.

3 Results and discussion

Due to the shorter interlayer distance and the partial ionic bonding between h-BN layers (i.e., lip–lip interactions), the exfoliation of h-BN is much more difficult than that of graphite [30]. Herein, to facilitate the exfoliation of h-BN, a novel strategy for chemically modifying the pristine h-BN is proposed, which is realized by soaking pristine h-BN in the $HClO_4$ solution for 10 h at a temperature of 180 °C. Figure 1(a) shows the FTIR spectrum of the $HClO_4$-soaked h-BN sample (BN-180). It can be seen that, besides an unimpressive peak near 3422 cm^{-1} which is due to the absorption of trace amounts of water on the surface of h-BN [31], both pristine h-BN and BN-180 exhibit two obvious absorption peaks at 1377 and 817 cm^{-1}, which belong to the in-plane B – N stretching vibration and the out-of-plane B – N – B bending vibration, respectively [32–33]. Distinctly different from that of h-BN, however, a visible peak occurs at 1049 cm^{-1} on the FTIR spectrum of the BN-180 sample, which is assigned to the symmetric B – O stretching (ν_1) band, demonstrating that BN-180 has been functionalized with oxygen functional groups [34]. Figure 1(b) displays XRD patterns of h-BN and BN-180 samples. It is seen that for both of them, there are five similar typical peaks at 26.6°, 41.4°, 43.8°, 50.0° and 53.18°, associated to (0 0 2), (1 0 0), (1 0 1), (1 0 2) and (0 0 4) planes of h-BN, respectively. It is worth noting that the (0 0 2) peak position of BN-180 shifts from 26.66° to 26.52°, indicating an increase in the interplanar distance ($d_{(0\,0\,2)}$) from 3.34 to 3.36 Å [35–36]. The $d_{(0\,0\,2)}$ increment ($\Delta d_{(0\,0\,2)}$) for BN-180 can be deduced to be 0.002 nm, which should be ascribed to the intercalation of $HClO_4$ between interlayers of h-BN during the long-term soaking process. This enlarged interlayer distance can also be clearly observed (Figs. 1(c) and 1(d)). So, we can conclude that the $HClO_4$-soaking can effectively expand the interlayer spacing of h-BN, which will facilitate its exfoliation into BNNS under the assistance of the MW irradiation.

Next, the BN-180 sample was soaked again in the $HClO_4$ solution at room temperature followed by the MW-irradiation and then the sonication, thus acquiring the exfoliated BNNS sample. Figure 2 shows typical morphological characteristics of the resultant BNNS sample. It can be clearly seen that the obtained BNNSs exhibit a wrinkled and semi-transparent film-like structure, demonstrating that BNNSs with the thin-layer structure have been successfully exfoliated from bulk h-BN [27].

Based on above results, the possible mechanism for the chemical exfoliation of h-BN may be deduced as follows: when pristine h-BN is soaked in the $HClO_4$ solution, the strong oxidizing property of $HClO_4$ will enable the edges

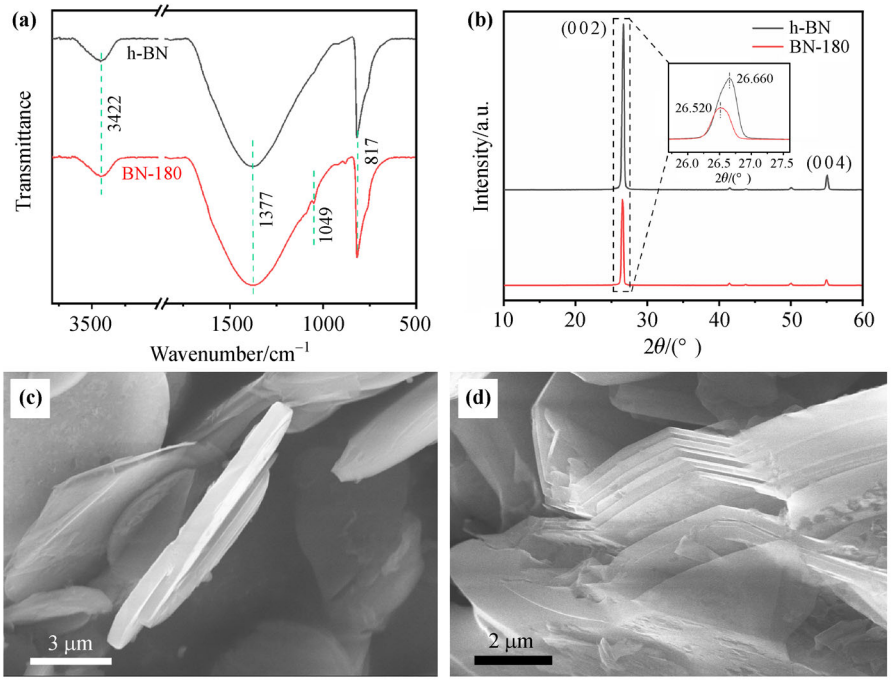

Fig. 1 Characterization of h-BN and BN-180: **(a)** FTIR spectra and **(b)** XRD patterns of pristine h-BN powders and BN-180; SEM images of **(c)** pristine h-BN and **(d)** BN-180.

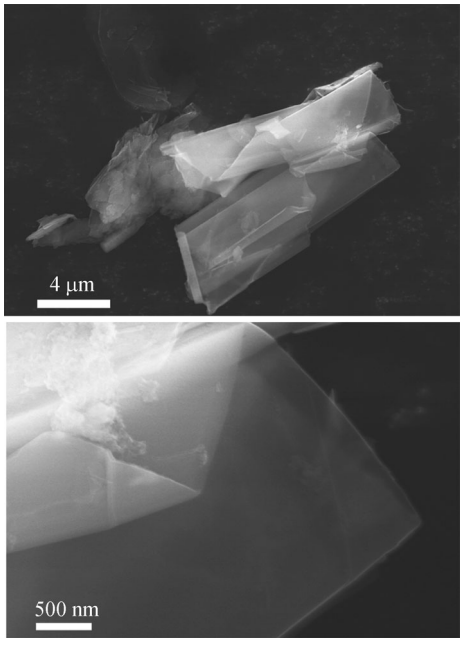

Fig. 2 SEM images of as-obtained BNNSs.

of h-BN to be oxidized (demonstrated by the FTIR characterization in Fig. 1(a)), resulting in the opening of h-BN edges. This edge-opening will facilitate $HClO_4$ to intercalate into interlayers between adjacent h-BN nanosheets, leading to a larger interlayer spacing of h-BN (as shown in Figs. 1(b) and 1(d)). When the soaked h-BN is soaked again in the $HClO_4$ solution, the larger interlayer spacing will allow more $HClO_4$ to intercalate among h-BN interlayer galleries, and the subsequent MW-irradiation will result in the rapid decomposition of introduced $HClO_4$ into gaseous substances (e.g., H_2O, O_2 and Cl_2), as shown in Eq. (1). Once the instantaneous gas pressure rise within the h-BN interlayer gallery can overcome the van der Waals force, the soaked h-BN will be effectively exfoliated into BNNSs. Figure 3 provides a schematic illustration of the fabrication mechanism of BNNSs. In addition, the analysis of products obtained under different reaction conditions (such as pre-soaking time and MW conditions) also proves that the proper pre-soaking time and sufficient gasification of $HClO_4$ under MW conditions are the basis for obtaining thin-layer structure BNNSs. This further validates the mechanism of the h-BN exfoliation proposed above from the side (Fig. S1, see the section on Supplementary information for detailed experimental description):

$$4HClO_4 \xrightarrow{\Delta} 2H_2O \uparrow +7O_2 \uparrow +2Cl_2 \uparrow \quad (2)$$

To further evaluate the as-obtained BNNS sample, the XRD characterization was performed, as shown in Fig. 4(a). Compared with that of pristine h-BN, the (0 0 2) peak of BNNSs shows a remarkably reduced intensity, implying its few-layer feature and significantly weaker stacking in the *c* direction [36–37]. Figure 4(b) further provides the Raman spectrum of the as-obtained BNNS sample. Clearly, the intensity of the G band of BNNSs is apparently weaker than that of bulk h-BN, and furthermore, the G band position of BNNSs shifts to 1366.8 cm^{-1} compared to that of h-BN (1365.0 cm^{-1}). These changes may suggest the reduction of h-BN layers [38–39]. To understand elemental compositions and chemical states of as-obtained BNNSs, the XPS measurement was conducted, as displayed in Figs. 4(c)–4(e). Chemical compositions of both BNNSs and h-BN are composed of B, N, O and C elements. For the h-BN sample, both B 1s and N 1s spectra can primarily be divided into a single peak centered at 190.5 and 398.1 eV, corresponding to the B – N bond and the N – B bond, respectively. As for the weak O 1s peak, it can be ascribed to the physically adsorbing moisture on the h-BN surface [40]. Different from those of h-BN, however, the high-resolution B 1s spectrum of BNNSs can be divided into two peaks located at 190.5 and 191.6 eV, corresponding to the B – N bond and the B – O bond, respectively. Similarly, the N 1s spectrum of BNNSs can be divided into two peaks located at 398.1 and 399.4 eV, which correspond to the N – B bond and the N – O bond, respectively [26,36,41]. The existence of B – O and N – O peaks demonstrates the introduction of oxygen into BNNSs during the MW-assisted chemical exfoliation process of h-BN.

Interestingly, no element Cl peak occurs on the XRS

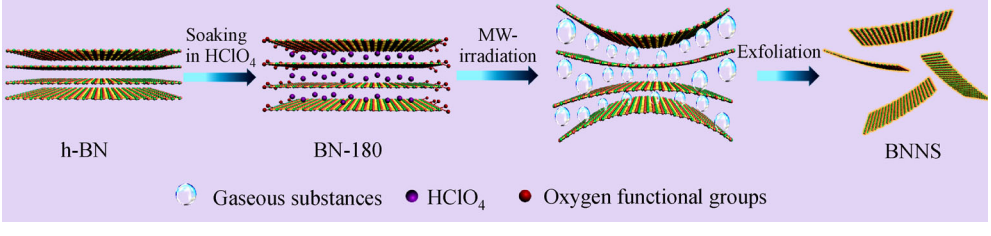

Fig. 3 Schematic illustration of the fabrication process of BNNSs.

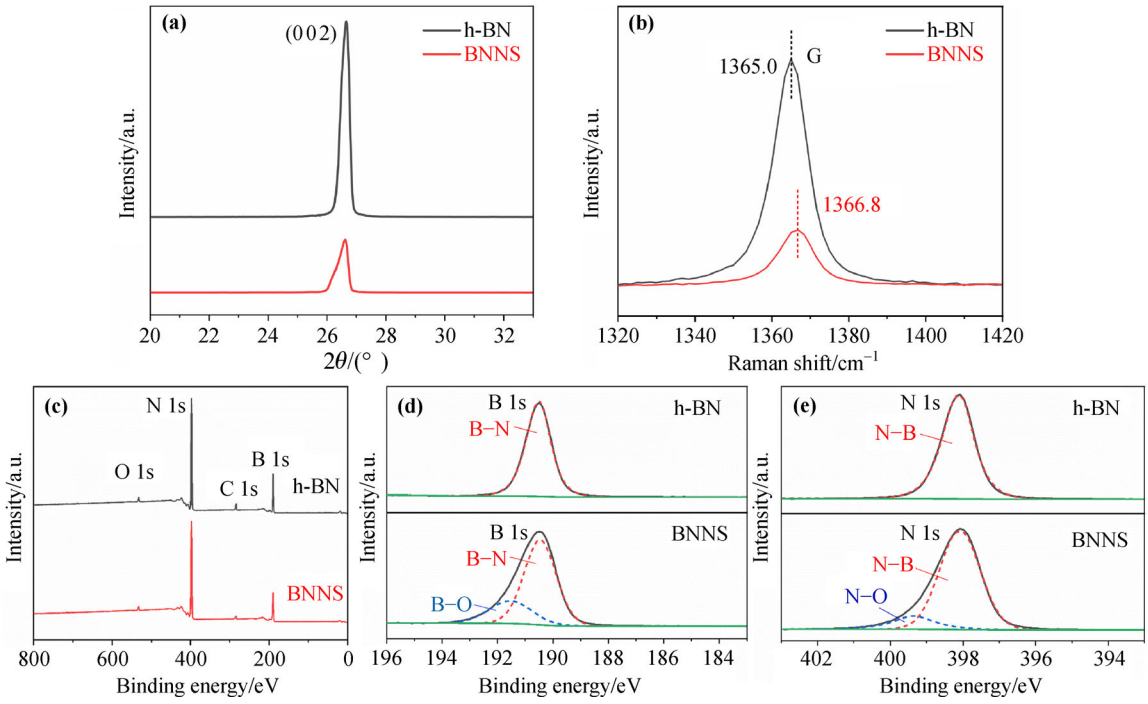

Fig. 4 Structural characterizations of h-BN and BNNSs: **(a)** XRD patterns; **(b)** Raman spectra; **(c)** XPS survey spectra; **(d)(e)** high-resolution XPS results of B 1s and N 1s.

spectrum of the BNNS sample, indicating that $HClO_4$ has been thoroughly decomposed and run away in a gaseous state from the BNNS sheets during microwave irradiation process. This non-existence of residual Cl on the BNNS sheets suggests that no water-washing procedure is needed, which will save a lot of water sources. Furthermore, the gaseous substances (e.g., Cl_2) resulting from the decomposition of $HClO_4$ can be collected for the production of sodium hypochlorite, aluminum trichloride, iron trichloride, etc. Therefore, the high-efficiency and less environmental impact will enable the present chemical exfoliation strategy to have more advantages than those conventional chemical exfoliation methods.

Figure 5(a) displays the typical TEM image of the BNNS sample. It can be clearly seen that the as-obtained BNNSs are highly transparent to the electron beam, indicating the ultrathin structure [42]. The high-resolution TEM (HR-TEM) image (Fig. 5(b)) further proves the existence of BNNS with a single layer, and the corresponding fast Fourier transformation (FFT) demonstrates the structural ordering of BNNSs, which suggests that there is no obvious damage to the structure of BNNSs during the chemical exfoliation process with $HClO_4$ [43]. To measure the lateral size and determine the size distribution of BNNSs, we deposited the as-obtained BNNS dispersion on the micro-grid for SEM observation, as shown in Fig. 5(c). Figure 5(d) illustrates the lateral size distribution of the obtained BNNS sample, which is inferred by randomly measuring the lateral size of 40 BNNS sheets. The calculated average lateral size of BNNS sheets is 7.1 μm, in which about 75% of sheets are more than 4 μm with a maximum lateral size of 16 μm. As far as we know, this average lateral size is much larger than those of 2D BNNSs obtained by using the top-down exfoliation methods reported previously (Table S1). In addition, the thickness of the obtained BNNSs is also evaluated by AFM. As shown in Figs. 5(e) and 5(f), the thickness of BNNSs is no more than 7 nm with an average thickness of 3.9 nm.

Large-size BNNSs prepared by this MW-assisted chemical exfoliation method are remarkably promising in various applications, especially as thermal conducting fillers to improve the thermal conductivity of polymer materials. To verify this, different PVA/BNNS composite films with BNNS contents of 0, 15, 25, 35, and 45 wt.% (denoted as PVA/BNNS-0, PVA/BNNS-15, PVA/BNNS-25, PVA/BNNS-35, and PVA/BNNS-45, respectively) were fabricated by a vacuum filtration method. Firstly, to understand the microstructure of the composite film, SEM observation was performed on a typical PVA/BNNS composite film with a BNNS content of 35 wt.%. As

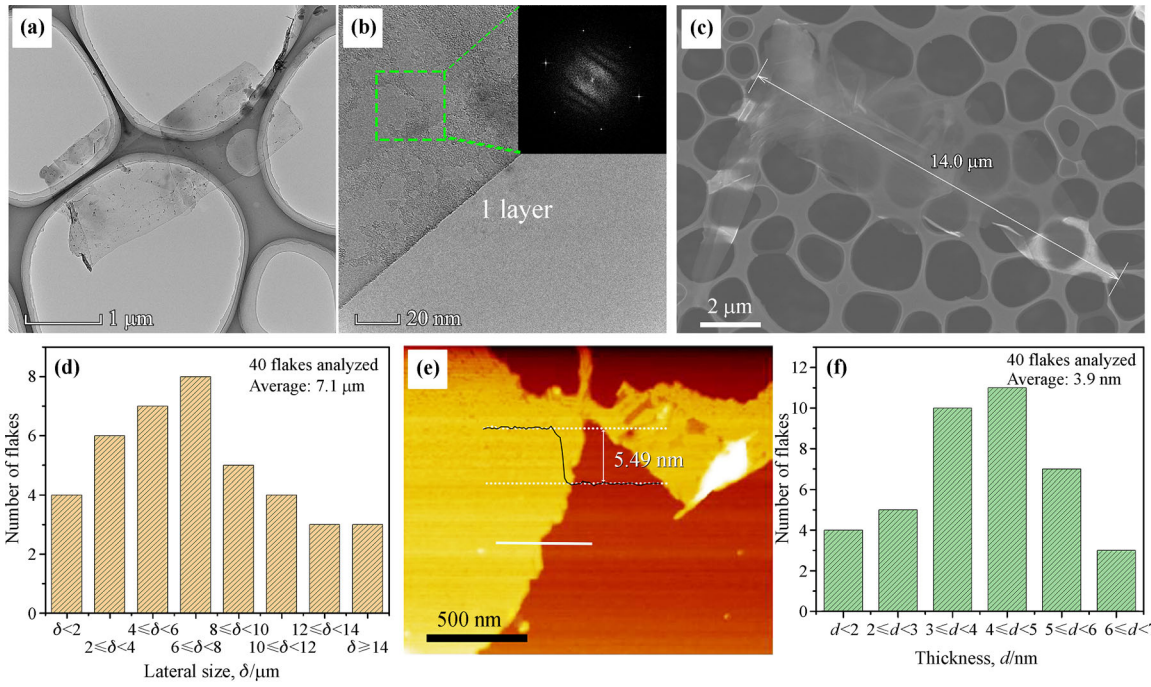

Fig. 5 Characterization of the obtained BNNSs: **(a)** typical TEM image; **(b)** HR-TEM and corresponding FFT images; **(c)** typical SEM image of BNNSs dispersed on the micro-grid; **(d)** lateral size distribution of BNNSs analyzed from 40 flakes; **(e)** typical AFM image; **(f)** thickness distribution analyzed by AFM statistics from 40 flakes.

displayed in Fig. 6(a), obviously, the composite film is composed of two parts. One part is an adhesive layer with PVA as the main component. The other part is the BNNS sample infiltrated with PVA, which has a densely arranged microstructure. From this, the preparation mechanism of the composite film can be deduced. Firstly, the 2D BNNS layers are easily aligned and closely lapped during the vacuum filtration process, thus forming a complete BNNS network, which is conducive to the construction of effective thermal conductivity paths. Then, with the addition of PVA, it can continuously penetrate between BNNS samples, but since the amount of PVA added is larger than the void volume between BNNS samples, a bonding layer is formed by the remaining PVA, which ensures the integrity of the composites. Moreover, the tensile stress–strain test was performed to understand mechanical properties of the composite films. Figure 6(b) shows the tensile stress–strain curves of PVA/BNNS composite films at various BNNS loadings. The tensile strength of PVA/BNNS-0 is 90.80 MPa with an elongation at break of 14.46%. After the embedment of BNNSs, both the tensile strength and the elongation at break of the films decreased with the filler content increase. When the BNNS loading reached 45 wt.%, these mechanical properties show a more significant drop compared with others. Detailed tensile properties can be found in Table S2. This decrease in mechanical properties may be due to the aggregation of BNNSs and the poor wettability between BNNSs and PVA. However, although the addition of BNNSs resulted in a decrease in mechanical properties of PVA, the PVA/BNNS composite films still exhibit excellent flexibility. As shown in Fig. 6(c), even with 35 wt.% BNNSs, the PVA/BNNS composite film obtained in this work can be repeatedly bent at a large bending angle of 180° for 100 times without causing any visible damage.

More importantly, it is advantageous for improving the thermal conductivity of the composites at which the BNNSs with large size and thin-layered structure can be easily prone to the orientation alignment with a low interfacial thermal resistance. Figure 6(d) displays the in-plane thermal diffusivity and the thermal conductivity of all composite films. The detailed properties (κ, α, ρ, and c) can be found in Table S3. Obviously, both the thermal diffusion coefficient and the thermal conductivity become higher with the increase of the BNNS fraction. The thermal diffusion coefficient and the thermal conductivity of pure PVA are 0.133 $mm^2 \cdot s^{-1}$ and 0.200 $W \cdot m^{-1} \cdot K^{-1}$, respectively. At the BNNS loading of 35 wt.%, the thermal diffusion coefficient and the thermal conductivity of the composite film increase to 6.813 $mm^2 \cdot s^{-1}$ and 12.416 $W \cdot m^{-1} \cdot K^{-1}$, which are 51 and 62 times higher than those of the pure PVA film, respectively. Furthermore, the resultant

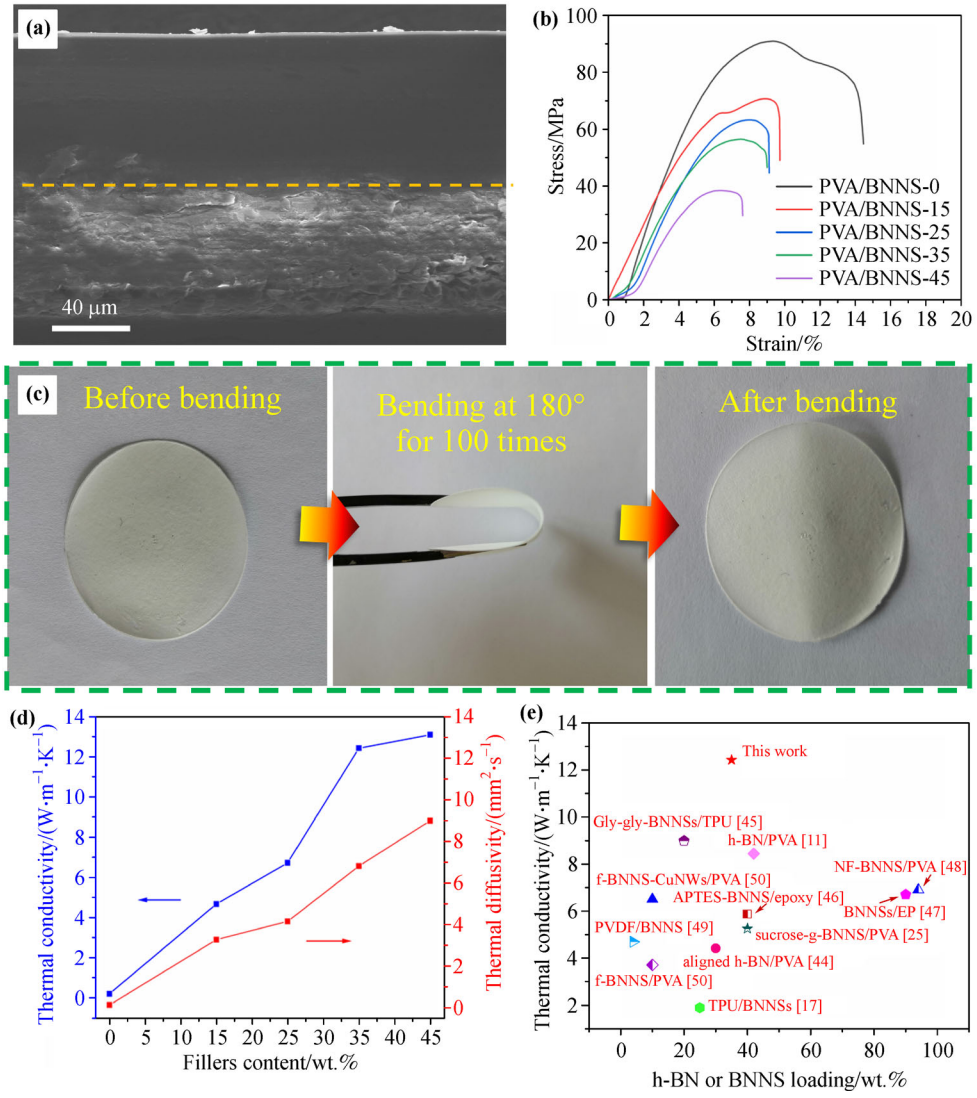

Fig. 6 **(a)** SEM image of the PVA/BNNS-35. **(b)** Tensile stress–strain curves of PVA/BNNS composite films with different loadings. **(c)** Photos of PVA/BNNS-35 before and after bending at 180° for 100 times. **(d)** The in-plane thermal diffusivity and conductivity of all films. **(e)** Comparison of thermal conductivity of the composite film in this work with BN-based composites reported in previous studies.

in-plane thermal conductivity of PVA/BNNS-45 is 13.082 $W \cdot m^{-1} \cdot K^{-1}$, slightly higher than that of PVA/BNNS-35. Since PVA/BNNS-35 behaves a slightly lower thermal conductivity but obviously a higher tensile strength, it should be more competent than the composites with over 35 wt.% filler content (e.g., PVA/BNNS-45) for the practical applications. The through-plane thermal conductivity of PVA/BNNS-35 was also measured, which is 0.933 $W \cdot m^{-1} \cdot K^{-1}$, much lower than that of the in-plane thermal conductivity of the film, indicating its good anisotropy. Finally, a comparative composite film with h-BN (the average thickness of 1 μm) as the filler (denoted as PVA/h-BN-35) was prepared by the same method to understand how the reduced thickness of BNNSs affects the thermal conductivity of the resultant composite. As shown in Fig. S2, the in-plane thermal conductivity of PVA/h-BN-35 is significantly lower than that of PVA/BNNS-35, suggesting that the reduced thickness of BNNSs is beneficial to the in-plane thermal conductivity of the resultant composite film. This may be due to the more consistent alignment orientation of thin-layer BNNSs during the compounding process compared to h-BN, which can facilitate the construction of a more complete in-plane heat conduction path to avoid the phonon scattering [15]. Figure 6(e) summarizes the thermal conductivity of BN-based polymer composites reported previously. Clearly, the PVA/BNNS composite film prepared in this work exhibits the highest thermal conductivity

[11,17,25,44–50], demonstrating that the large-size BNNSs obtained by the present strategy is very promising for the improvement of the thermal conductivity of polymer materials.

4 Conclusions

In summary, a facile yet efficient MW-assisted chemical method has been proposed for scalable preparation of BNNSs with the large-size and thin-layer structure. In this method, $HClO_4$ is used as the only reagent to oxidize edges of h-BN and intercalate among interlayer galleries to weaken the interlayer interaction force of h-BN. The subsequent MW irradiation leads to the rapid decomposition of the intercalated $HClO_4$ and thereby the effective exfoliation of h-BN. The average thickness of BNNSs obtained by this method is 3.9 nm, behaving a thin-layered structure. More interestingly, the average size of resultant BNNSs is up to 7.1 μm, which is, to the best of our knowledge, among the highest values so far reported for top-down exfoliated BNNSs. Benefiting from the large size, the prepared BNNSs have great potential in improving the thermal conductivity of polymer materials. When BNNSs as the thermal conducting filler are composited with PVA, the as-prepared PVA/BNNS composite exhibits a dramatic enhancement in the thermal conductivity compared with pure PVA. Moreover, the high efficiency and less environmental impact will enable the present chemical exfoliation strategy more competent in the scalable preparation of large-size BNNSs than those conventional chemical exfoliation methods.

Disclosure of potential conflicts of interest The authors declare that they have no conflict of interest.

Acknowledgements Projects 52172052 and 51872253 supported by the National Natural Science Foundation of China and Project E2019203480 supported by the Hebei Natural Science Foundation of China.

References

[1] Moore A L, Shi L. Emerging challenges and materials for thermal management of electronics. Materials Today, 2014, 17(4): 163–174

[2] Lancaster A, Keswani M. Integrated circuit packaging review with an emphasis on 3D packaging. Integration, 2018, 60: 204–212

[3] Tan C, Dong Z, Li Y, et al. A high performance wearable strain sensor with advanced thermal management for motion monitoring. Nature Communications, 2020, 11(1): 3530

[4] Feng C P, Chen L B, Tian G L, et al. Multifunctional thermal management materials with excellent heat dissipation and generation capability for future electronics. ACS Applied Materials & Interfaces, 2019, 11(20): 18739–18745

[5] Feng C P, Chen L B, Tian G L, et al. Robust polymer-based paper-like thermal interface materials with a through-plane thermal conductivity over 9 $W\cdot m^{-1}\cdot K^{-1}$. Chemical Engineering Journal, 2020, 392: 123784

[6] Yu C, Gong W, Tian W, et al. Hot-pressing induced alignment of boron nitride in polyurethane for composite films with thermal conductivity over 50 $W\cdot m^{-1}\cdot K^{-1}$. Composites Science and Technology, 2018, 160: 199–207

[7] Zhang Z, Qu J, Feng Y, et al. Assembly of graphene-aligned polymer composites for thermal conductive applications. Composites Communications, 2018, 9: 33–41

[8] Singh S, Shervin S, Sun H, et al. Using mosaicity to tune thermal transport in polycrystalline aluminum nitride thin films. ACS Applied Materials & Interfaces, 2018, 10(23): 20085–20094

[9] Morishita T, Matsushita M, Katagiri Y, et al. A novel morphological model for carbon nanotube/polymer composites having high thermal conductivity and electrical insulation. Journal of Materials Chemistry, 2011, 21(15): 5610–5614

[10] Yu C, Zhang J, Li Z, et al. Enhanced through-plane thermal conductivity of boron nitride/epoxy composites. Composites Part A: Applied Science and Manufacturing, 2017, 98: 25–31

[11] Zhang J, Wang X, Yu C, et al. A facile method to prepare flexible boron nitride/poly (vinyl alcohol) composites with enhanced thermal conductivity. Composites Science and Technology, 2017, 149: 41–47

[12] Song W L, Wang P, Cao L, et al. Polymer/boron nitride nanocomposite materials for superior thermal transport performance. Angewandte Chemie, 2012, 124(26): 6604–6607

[13] Zhang K, Feng Y, Wang F, et al. Two dimensional hexagonal boron nitride (2D-hBN): synthesis, properties and applications. Journal of Materials Chemistry C: Materials for Optical and Electronic Devices, 2017, 5(46): 11992–12022

[14] Chen J, Huang X, Zhu Y, et al. Cellulose nanofiber supported 3D interconnected BN nanosheets for epoxy nanocomposites with ultrahigh thermal management capability. Advanced Functional Materials, 2017, 27(5): 1604754

[15] Zhu Z, Li C, Songfeng E, et al. Enhanced thermal conductivity of polyurethane composites via engineering small/large sizes interconnected boron nitride nanosheets. Composites Science and Technology, 2019, 170: 93–100

[16] Lin Z, Mcnamara A, Liu Y, et al. Exfoliated hexagonal boron nitride-based polymer nanocomposite with enhanced thermal conductivity for electronic encapsulation. Composites Science and

Technology, 2014, 90: 123–128

[17] Yuan F, Jiao W, Yang F, et al. Scalable exfoliation for large-size boron nitride nanosheets by low temperature thermal expansion-assisted ultrasonic exfoliation. Journal of Materials Chemistry C: Materials for Optical and Electronic Devices, 2017, 5(25): 6359–6368

[18] Joy J, George E, Haritha P, et al. An overview of boron nitride based polymer nanocomposites. Journal of Polymer Science, 2020, 58(22): 3115–3141

[19] Khan M H, Liu H K, Sun X, et al. Few-atomic-layered hexagonal boron nitride: CVD growth, characterization, and applications. Materials Today, 2017, 20(10): 611–628

[20] Zhi C, Bando Y, Tang C, et al. Large-scale fabrication of boron nitride nanosheets and their utilization in polymeric composites with improved thermal and mechanical properties. Advanced Materials, 2009, 21(28): 2889–2893

[21] Wang X, Yang Y, Jiang G, et al. A facile synthesis of boron nitride nanosheets and their potential application in dye adsorption. Diamond and Related Materials, 2018, 81: 89–95

[22] Jung J H, Park C H, Ihm J. A rigorous method of calculating exfoliation energies from first principles. Nano Letters, 2018, 18 (5): 2759–2765

[23] Lin Y, Williams T V, Xu T B, et al. Aqueous dispersions of few-layered and monolayered hexagonal boron nitride nanosheets from sonication-assisted hydrolysis: critical role of water. The Journal of Physical Chemistry C, 2011, 115(6): 2679–2685

[24] Deshmukh A R, Jeong J W, Lee S J, et al. Ultrasound-assisted facile green synthesis of hexagonal boron nitride nanosheets and their applications. ACS Sustainable Chemistry & Engineering, 2019, 7(20): 17114–17125

[25] Chen S, Xu R, Liu J, et al. Simultaneous production and functionalization of boron nitride nanosheets by sugar-assisted mechanochemical exfoliation. Advanced Materials, 2019, 31(10): 1804810

[26] Lei W, Mochalin V N, Liu D, et al. Boron nitride colloidal solutions, ultralight aerogels and freestanding membranes through one-step exfoliation and functionalization. Nature Communications, 2015, 6: 8849

[27] Bhimanapati G R, Kozuch D, Robinson J A. Large-scale synthesis and functionalization of hexagonal boron nitride nanosheets. Nanoscale, 2014, 6(20): 11671–11675

[28] Zhao H R, Ding J H, Shao Z Z, et al. High-quality boron nitride nanosheets and their bioinspired thermally conductive papers. ACS Applied Materials & Interfaces, 2019, 11(40): 37247–37255

[29] Du M, Wu Y, Hao X. A facile chemical exfoliation method to obtain large size boron nitride nanosheets. CrystEngComm, 2013, 15(9): 1782–1786

[30] Lee D, Lee B, Park K H, et al. Scalable exfoliation process for highly soluble boron nitride nanoplatelets by hydroxide-assisted ball milling. Nano Letters, 2015, 15(2): 1238–1244

[31] Hou J, Li G, Yang N, et al. Preparation and characterization of surface modified boron nitride epoxy composites with enhanced thermal conductivity. RSC Advances, 2014, 4(83): 44282–44290

[32] Cui Z, Oyer A J, Glover A J, et al. Large scale thermal exfoliation and functionalization of boron nitride. Small, 2014, 10(12): 2352–2355

[33] Geick R, Perry C H, Rupprecht G. Normal modes in hexagonal boron nitride. Physical Review, 1966, 146(2): 543–547

[34] Sainsbury T, Satti A, May P, et al. Oxygen radical functionalization of boron nitride nanosheets. Journal of the American Chemical Society, 2012, 134(45): 18758–18771

[35] Zhu W, Gao X, Li Q, et al. Controlled gas exfoliation of boron nitride into few-layered nanosheets. Angewandte Chemie, 2016, 128(36): 10924–10928

[36] Cheng Z L, Ma Z S, Ding H L, et al. Environmentally friendly, scalable exfoliation for few-layered hexagonal boron nitride nanosheets (BNNSs) by multi-time thermal expansion based on released gases. Journal of Materials Chemistry C: Materials for Optical and Electronic Devices, 2019, 7(46): 14701–14708

[37] Chao Y, Liu M, Pang J, et al. Gas-assisted exfoliation of boron nitride nanosheets enhancing adsorption performance. Ceramics International, 2019, 45(15): 18838–18843

[38] Li L H, Cervenka J, Watanabe K, et al. Strong oxidation resistance of atomically thin boron nitride nanosheets. ACS Nano, 2014, 8 (2): 1457–1462

[39] Gorbachev R V, Riaz I, Nair R R, et al. Hunting for monolayer boron nitride: optical and Raman signatures. Small, 2011, 7(4): 465–468

[40] Li X, Hao X, Zhao M, et al. Exfoliation of hexagonal boron nitride by molten hydroxides. Advanced Materials, 2013, 25(15): 2200–2204

[41] Cao C, Xue Y, Liu Z, et al. Scalable exfoliation and gradable separation of boric-acid-functionalized boron nitride nanosheets. 2D Materials, 2019, 6(3): 035014

[42] Zhu M, Li G, Zhang X, et al. High yield and concentration exfoliation of defect-free 2D nanosheets via gentle water freezing-thawing approach and stabilization with PVP. Materials Research Express, 2019, 6(11): 1150c9

[43] Zhang C, Tan J, Pan Y, et al. Mass production of 2D materials by intermediate-assisted grinding exfoliation. National Science Review, 2020, 7(2): 324–332

[44] Xie B H, Huang X, Zhang G J. High thermal conductive polyvinyl alcohol composites with hexagonal boron nitride microplatelets as fillers. Composites Science and Technology, 2013, 85: 98–103

[45] E S, Zhu Z, Xie L, et al. An integrated strategy towards the high-yield fabrication of soluble boron nitride nanosheets. Chemical Engineering Journal, 2019, 360: 1407–1415

[46] Liu Z, Li J, Liu X. Novel functionalized BN nanosheets/epoxy

composites with advanced thermal conductivity and mechanical properties. ACS Applied Materials & Interfaces, 2020, 12(5): 6503–6515

[47] Fu K, Yang J, Cao C, et al. Highly multifunctional and thermoconductive performances of densely filled boron nitride nanosheets/epoxy resin bulk composites. ACS Applied Materials & Interfaces, 2021, 13(2): 2853–2867

[48] Zeng X, Ye L, Yu S, et al. Artificial nacre-like papers based on noncovalent functionalized boron nitride nanosheets with excellent mechanical and thermally conductive properties. Nanoscale, 2015, 7(15): 6774–6781

[49] Wang M, Jiao Z, Chen Y, et al. Enhanced thermal conductivity of poly(vinylidene fluoride)/boron nitride nanosheet composites at low filler content. Composites Part A: Applied Science and Manufacturing, 2018, 109: 321–329

[50] Yin C G, Liu Z J, Mo R, et al. Copper nanowires embedded in boron nitride nanosheet-polymer composites with enhanced thermal conductivities for thermal management. Polymer, 2020, 195: 122455

Supplementary information

In order to further understand the influence of different reaction conditions such as pre-soaking time and MW conditions on the morphology and thickness of the resulting product, the SEM characterization was performed. As seen in Figs. S1(a) and S1(b), the samples obtained without pre-soaking (BNNS-0) show a thickness and morphology similar to the original h-BN and no flake-like BNNSs was observed. However, it is worth noting that part of the lamella curling can be observed on the edges of some samples. This may be due to the lack of an effective process of $HClO_4$ intercalation, resulting in $HClO_4$ gasification occurred only at the edge of h-BN during the MW heating process. When the pre-soaking time was 5 h, the morphology of the obtained sample (BNNS-5) changed significantly compared with h-BN, and some translucent flakes started to peel off from the edge of h-BN (Figs. S1(c) and S1(d)). This may be caused by insufficient intercalation during the pre-soaking process, so that only part of the h-BN peeled off during the MW heating process. Further extending the pre-soaking time to 15 h, BNNSs with large translucent flakes could be clearly observed (Figs. S1(e) and S1(f)), and the yield of BNNSs (16.8%) did not change significantly compared with the pre-soaking time of 10 h. This indicates that sufficient intercalation of h-BN has been achieved at the pre-soaking time of 10 h, and further extending the time would not have a significant effect on the results.

In addition, to verify the effect of MW conditions on BNNSs, the pre-soaking time was set to 10 h, while the MW time was shortened to only 3 min (labeled as BNNS-3MW). As shown in Figs. S1(g) and S1(h), interestingly, unlike h-BN, some BNNS-3MW exhibited a larger void structure between layers but did not undergo complete exfoliation, probably because $HClO_4$ fully intercalated into h-BN was only partially vaporized during the insufficient MW time, which was not sufficient to allow complete exfoliation of h-BN.

In general, it can be seen from the above experimental results that proper pre-soaking time and microwave

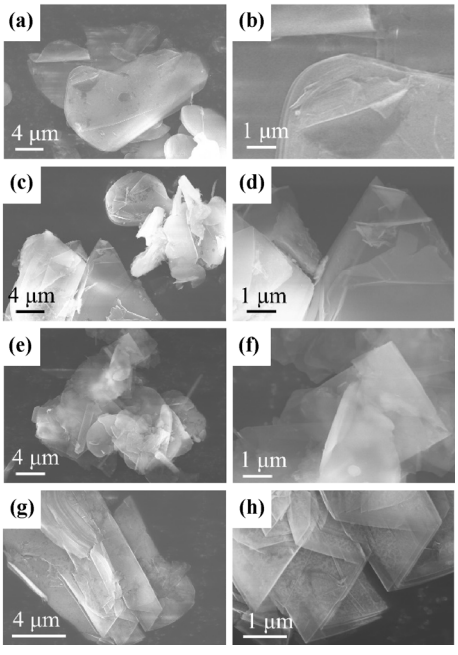

Fig. S1 SEM images of the products obtained under different experimental conditions: **(a)(b)** BNNS-0; **(c)(d)** BNNS-5; **(e)(f)** BNNS-15; **(g)(h)** BNNS-3MW.

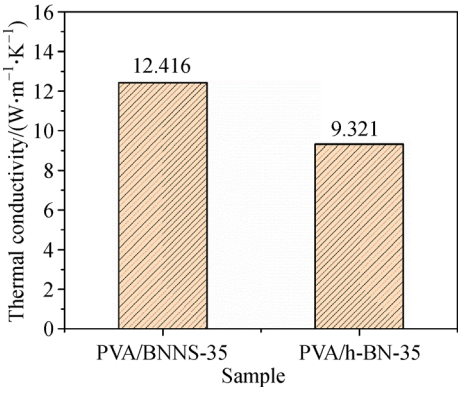

Fig. S2 Comparison of in-plan thermal conductivities of composite films with BNNSs and h-BN as fillers, respectively.

conditions are essential for the exfoliation of h-BN, that is, sufficient pre-soaking treatment can make h-BN fully intercalate by $HClO_4$, and subsequent MW heating causes $HClO_4$ between the layers to rapidly decompose into gaseous state and generate a driving force along the *c*-axis of h-BN, resulting in BNNSs with a thin layer structure.

Table S1 Comparison of the lateral size of BNNSs obtained by various exfoliation methods [S1–S13]

Exfoliation method	Specific operation	Lateral size/μm	Yield/%	Ref.
Liquid-phase sonication	Sonication in DMF	< 1	0.05–0.1	[S1]
	Sonication in deionized water	< 1	< 5	[S2]
	Sonication in NMP-salt solutions	0.1	15	[S3]
	Sonication in various extracts of plant materials	0.0777	~23	[S4]
Ball milling	Sugar-assisted ball milling	0.089	87.3	[S5]
	Urea-assisted ball milling	~0.1	85	[S6]
	β-Cyclodextrin-assisted ball milling	0.5–1	60	[S7]
Chemical exfoliation	Exfoliation by H_2 induced thermal expansion	1.6	26	[S8]
	Exfoliation by H_2SO_4 intercalated	0.6	15	[S9]
	Exfoliation by a modified Hummers' method	~3	6.5	[S10]
	Chemical exfoliation in acid mixture	1–3	–	[S11]
Others	Gas exfoliation in liquid N_2	0.05–0.50	16–20	[S12]
	Intermediate-assisted grinding exfoliation	1.2	67	[S13]
	MW-assisted chemical exfoliation	7.1	~16	this work

Table S2 Tensile properties of the composite films with different mass fractions of BNNS fillers

Mass fraction/wt.%	Tensile strength/MPa	Elongation at break/%
0	90.80	14.46
15	70.62	9.73
25	63.15	9.12
35	56.35	9.01
45	38.29	7.62

Table S3 Physical properties of composite films with different mass fractions of BNNS fillers

Mass fraction/wt.%	Density/($g \cdot cm^{-3}$)	Specific heat/($J \cdot g^{-1} \cdot K^{-1}$)	Thermal diffusivity/($mm^2 \cdot s^{-1}$)	Thermal conductivity/($W \cdot m^{-1} \cdot K^{-1}$)
0	0.833	1.808	0.133	0.200
15	1.062	1.346	3.266	4.669
25	1.203	1.350	4.143	6.728
35	1.352	1.348	6.813	12.416
45	1.411	1.032	8.984	13.082

References

[S1] Zhi C, Bando Y, Tang C, et al. Large-scale fabrication of boron nitride nanosheets and their utilization in polymeric composites with improved thermal and mechanical properties. Advanced Materials, 2009, 21(28): 2889–2893

[S2] Lin Y, Williams T V, Xu T B, et al. Aqueous dispersions of few-layered and monolayered hexagonal boron nitride nanosheets from sonication-assisted hydrolysis: critical role of water. The Journal of Physical Chemistry C, 2011, 115(6): 2679–2685

[S3] Wang H, Su X, Song T, et al. Scalable exfoliation and dispersion of few-layer hexagonal boron nitride nanosheets in NMP-salt solutions. Applied Surface Science, 2019, 488: 656–661

[S4] Deshmukh A R, Jeong J W, Lee S J, et al. Ultrasound-assisted facile green synthesis of hexagonal boron nitride nanosheets and their applications. ACS Sustainable Chemistry & Engineering, 2019, 7(20): 17114–17125

[S5] Chen S, Xu R, Liu J, et al. Simultaneous production and functionalization of boron nitride nanosheets by sugar-assisted mechanochemical exfoliation. Advanced Materials, 2019, 31(10): 1804810

[S6] Lei W, Mochalin V N, Liu D, et al. Boron nitride colloidal solutions, ultralight aerogels and freestanding membranes through one-step exfoliation and functionalization. Nature Communications, 2015, 6(1): 1–8

[S7] Ji D, Wang Z, Zhu Y, et al. One-step environmentally friendly exfoliation and functionalization of hexagonal boron nitride by β-cyclodextrin-assisted ball milling. Ceramics International, 2020, 46

(13): 21084–21089

[S8] Yuan F, Jiao W, Yang F, et al. Scalable exfoliation for large-size boron nitride nanosheets by low temperature thermal expansion-assisted ultrasonic exfoliation. Journal of Materials Chemistry C, 2017, 5(25): 6359–6368

[S9] Wang X, Yang Y, Jiang G, et al. A facile synthesis of boron nitride nanosheets and their potential application in dye adsorption. Diamond and Related Materials, 2018, 81: 89–95

[S10] Du M, Wu Y, Hao X. A facile chemical exfoliation method to obtain large size boron nitride nanosheets. CrystEngComm, 2013, 15(9): 1782–1786

[S11] Gao W, Zhao Y, Yin H. Lateral size selection of liquid exfoliated hexagonal boron nitride nanosheets. RSC Advances, 2018, 8(11): 5976–5983

[S12] Zhu W, Gao X, Li Q, et al. Controlled gas exfoliation of boron nitride into few-layered nanosheets. Angewandte Chemie, 2016, 128(36): 10924–10928

[S13] Zhang C, Tan J, Pan Y, et al. Mass production of 2D materials by intermediate-assisted grinding exfoliation. National Science Review, 2020, 7(2): 324–332